

NMR evidence for an antisite-induced magnetic moment on Bi in a topological insulator heterostructures $\text{MnBi}_2\text{Te}_4/(\text{Bi}_2\text{Te}_3)_n$

R. Kalvig, E. Jedryka, A. Lynnyk, P. Skupiński, K. Graszka, and M. Wójcik
*Institute of Physics, Polish Academy of Sciences,
 Aleja Lotników 32/46, Warsaw, PL-02668, Poland*
 (Dated: August 22, 2025)

MnBi_2Te_4 (MBT) is the first intrinsic magnetic topological insulator, combining a topologically protected surface metallic state and intrinsic magnetic order. A structural compatibility with the nonmagnetic Bi_2Te_3 (BT) parent compound gives a possibility to create MBT/BT heterostructures and manipulate their magnetic state in view of optimizing the Quantum Anomalous Hall Effect (QAHE). In this work an extensive NMR study, supported by the bulk magnetization measurements has been performed at 4.2 K on a self-organized single crystal $\text{MnBi}_2\text{Te}_4/(\text{Bi}_2\text{Te}_3)_n$ heterostructure. ^{55}Mn and ^{209}Bi NMR signals have been recorded as a function of the out-of-plane magnetic field up to 6 T, covering a spin-flop transition from the antiferromagnetic (AFM) to the canted antiferromagnetic (CAFM) configuration of the Mn layers. Structural defects were shown to contribute a small ferromagnetic component below the spin-flop field. Presence of the AFM-coupled Mn antisites has been evidenced and shown to induce an antiparallel magnetic moment on Bi atoms within the host Bi layer. Detection of the induced magnetic moment on bismuth which contributes a new ferromagnetic component is of utmost importance for understanding the magnetic interactions in the MBT/BT system. These findings have potentially important implications for engineering the QAH devices.

Magnetically ordered topological insulators have attracted a great deal of attention during last decade. A combination of topologically protected surface metallic state and intrinsic magnetic order provides excellent ground for investigating Axion Insulating States and Quantum Anomalous Hall Effect (QAHE) [1, 2]. The possibility of realizing QAHE in zero external magnetic field is particularly sought after as a bridge to develop low power consumption materials and devices [3–5]. Following several theoretical predictions and first experimental confirmation it has been demonstrated that that MnBi_2Te_4 – the first intrinsic magnetic topological insulator – is a great platform to investigate those elusive physical phenomena [6–14].

MnBi_2Te_4 (often referred to as MBT) crystallizes in a rhombohedral layered structure with the space group $R\bar{3}m$ and has the following lattice parameters $a = 4.332$ Å and $c = 42.979$ Å [15]. It is a derivative of Bi_2Te_3 – an intensely studied non-magnetic topological insulator. In MnBi_2Te_4 the hexagonally arranged monoatomic layers are stacked along the c-direction [0001] in the sequence Te – Bi – Te – Mn – Te – Bi – Te, forming a septuple layer blocks (SL) as shown in Fig. 1(a). The subsequent SLs are weakly bonded by van der Waals forces, giving a possibility of interlacing the SL blocks with several layers of an isostructural Bi_2Te_3 . Such heterostructures – denoted as $\text{MnBi}_2\text{Te}_4/(\text{Bi}_2\text{Te}_3)_n$ exhibit a variety of the long-range magnetic ordering, creating a tunable platform of different topological states of matter [16, 17]. They consist of the magnetic septuplets (SLs) alternating with non-magnetic quintuple layers (QLs) of Bi_2Te_3 (Te – Bi – Te – Bi – Te). The n number in the formula denotes a number of the QLs separating the subsequent SLs.

Structurally perfect MnBi_2Te_4 ($n = 0$) is an A-type

antiferromagnet along the c-axis [0001] with a transition temperature $T_N = 24$ K [7, 18]. Within each septuplet the layers of Mn atoms are ferromagnetically (FM) ordered along the easy c-axis and are antiferromagnetically (AFM) coupled to the Mn layer in the neighbor SL. The AFM coupling persist also when the subsequent SLs are separated by one or two QLs, whereas for $n \geq 3$ the antiferromagnetic interaction is not active anymore [16]. The AFM coupling can also be broken by application of the external magnetic field along the [0001] direction: a spin-flop transition has been observed near 3.57 T at 2 K leading to a metastable canted AFM (CAFM) state [19]. It has recently been shown that a self-organized growth is a preferable way to achieve the $\text{MnBi}_2\text{Te}_4/(\text{Bi}_2\text{Te}_3)_n$ heterostructures, giving materials that are magnetically better organized than the substitutional Mn-doping of the Bi_2Te_3 crystals [20]. This preparation method has an advantage of achieving a considerable volume of a material in form of a single crystal, but does not allow to control precisely the distribution of the QLs, so the n number reveals a certain distribution over the sample volume. Other potential structural defects include a magnetic disorder within SLs in form of Mn_{Bi} and Bi_{Mn} antisites as well as Mn/Bi intermixing within QLs [20]. The structural defects lead to the onset of alien magnetic interactions, and have a deteriorating effect on the QAHE state [17, 21, 22], stressing the importance of understanding the role they play in the system.

Nuclear Magnetic Resonance (NMR) experiment is an invaluable tool to disentangle the magnetic response and identify different magnetic phases present in a multiphase magnetic system, since it is a site-sensitive and element-sensitive probe. The experiment involves the entire volume of the material providing a distribution of intrinsic local magnetic fields that depend on a magnetic state of

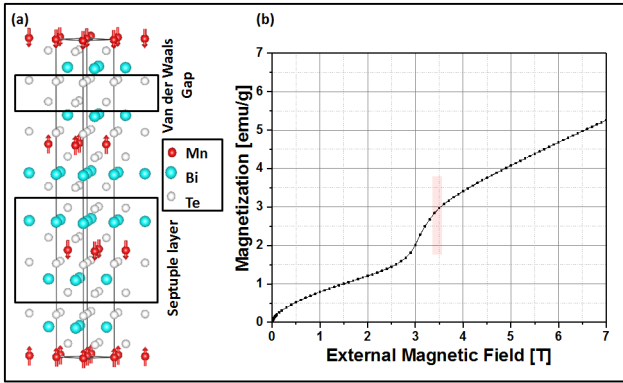


FIG. 1: (a) Schematic magnetic structure of the MnBi_2Te_4 . Mn atoms self-organize as a central layer within a septuplet (Te – Bi – Te – Mn – Te – Bi – Te) and reveal FM order. Magnetic moments (represented here by red vectors) are AFM coupled to the subsequent Mn-planes. Bi and Te atoms are represented with full cyan and white open circles, respectively. This drawing was prepared by means of VESTA software [23]. (b) Experimental magnetization curve of an inhomogeneous $\text{MnBi}_2\text{Te}_4/(\text{Bi}_2\text{Te}_3)_n$ heterostructure measured at 4.2 K. with the external magnetic field applied along [0001] direction. Spin – flop transition reported to take place in MBT between 3.4 T [11] and 3.57 T [19] is highlighted.

a probed atom and its interaction with the magnetic environment. In this work we have used it to shed some light on the local structural and magnetic properties of a self-organized $\text{MnBi}_2\text{Te}_4/(\text{Bi}_2\text{Te}_3)_n$ single crystal, where n is the number of QLs separating SLs which in our case is $n = 2$ on average as determined from the TEM image. The NMR spectra have been recorded at different values of the external magnetic field and analyzed in the context of bulk magnetization measurements. A well-defined orientation of the magnetic field versus the crystal axes made it possible to follow the spin flop transition to the CAFM state and investigate the orientation of the manganese antisite magnetic moments. Most importantly, this study provides the first direct experimental evidence for an antisite – induced magnetic moment on Bi atoms.

The sample under study was a single crystal obtained by the Bridgman growth process from the $\text{Mn}_{0.81}\text{Bi}_{2.06}\text{Te}_{4.13}$ melt and no chemical inhomogeneity has been observed by means of energy dispersive x-ray analysis. The details of sample preparation and initial characterization have been described in ref. [20]. NMR experiments were performed using an automatic, phase-sensitive spin-echo spectrometer with a tunable probe [24]. ^{209}Bi and ^{55}Mn resonances have been investigated at 4.2 K by sweeping frequency in the range 60 – 200 MHz and 350 – 440 MHz, with a step of 1 MHz. The external magnetic field was applied along the c-axis (i.e. [0001] direction) of the studied crystal and varied in the range 0–6 T. Experimental NMR spectra have been corrected for the NMR enhancement factor using the Panisod protocol [25]. Macroscopic magnetic characterization was carried out with a Quantum Design superconducting quantum interference device magnetometer (SQUID) at

a constant temperature of 4 K.

The magnetic structure expected for the perfectly ordered $\text{MnBi}_2\text{Te}_4/(\text{Bi}_2\text{Te}_3)_n$ system [7, 9] is presented in the Fig. 1(a), whereas Fig. 1(b) presents the results of macroscopic magnetization measurements performed on the studied sample vs. the external magnetic field up to 7 T applied along the [0001] direction (i.e. perpendicular to the Mn planes). Unlike the M vs H curves reported for the purely antiferromagnetic MnBi_2Te_4 , where magnetization is close to zero below the spin flop transition (SFT) reported to take place between 3.4 T and 3.57 T [7, 11, 19, 26], we observe at lower fields an uncompensated ferromagnetic contribution similar to that reported in previous studies of the $\text{MnBi}_2\text{Te}_4/(\text{Bi}_2\text{Te}_3)_n$ systems [20–22, 27] and attributed to disorder effects. These include on one hand a certain distribution of distances between the neighbour SLs (i.e. a variation of the n number across the sample). In those parts of a sample where the SLs are separated by three or more QLs the AFM coupling is not active [16] and their magnetic moments easily align along the external field. On the other hand, Mn atoms can replace Bi atoms in QLs while Bi can substitute Mn in the Mn layers [21, 22, 28]. These Mn antisites within QLs effects were reported to couple ferromagnetically to the Mn layers within SLs [20, 27, 29] and may also contribute to the observed uncompensated magnetic contribution. In the field range 2.5 – 3.5 T we observe a rapid growth of magnetization due to a spin flop transition and an onset of a canted AFM (CAFM) configuration, in consistence with previous literature reports [7, 11, 19, 26]. A non-sharp character of this transition reflects a certain distribution of the AFM coupling strength between the different SLs. Above 3.5 T, a further linear increase of magnetization is observed, related to the rotation of canted spins towards the c-axis. The magnetic saturation is not reached within the available magnetic field range (0–7 T), in line with the previously reported data showing that the MBT system requires around 60 T to reach magnetic saturation [30]. This macroscopic magnetic characterization will serve as a basis to understand the details of the NMR results.

Figure 2(a) presents the ^{55}Mn NMR spectra recorded at 4.2 K at different values of the external magnetic field applied along the [0001] direction, i.e., along the crystallographic c-axis. First, we note the presence of two distinct spectrum components (here marked as red and black, respectively), their frequency shifting in opposite directions with increasing magnetic field strength. The frequency position of their gravity center is plotted in Fig. 2(b) as a function of external magnetic field. At zero field we observe only one spectrum component (red line), centered around 419 MHz. With increasing external field this signal shifts towards higher frequencies reaching 435 MHz at 2 T. Beyond 2 T the “red” signal intensity rapidly drops. On the other hand the “black” spectrum component comes into picture only at 1.5 T increasing in intensity up to 3.5 T while its frequency position reveals a continuous downshift in the entire in-

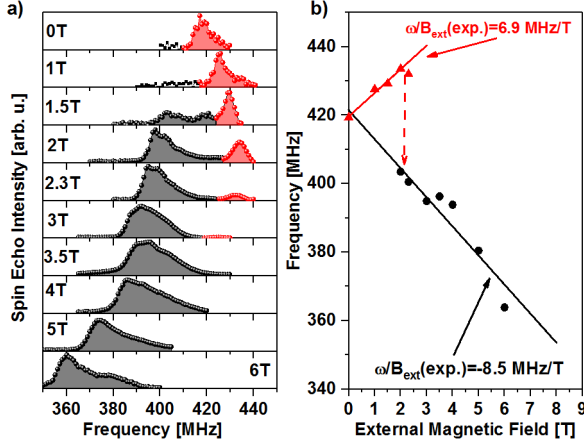


FIG. 2: (a) ^{55}Mn NMR spectra recorded at 4.2 K from an inhomogeneous $\text{MnBi}_2\text{Te}_4/(\text{Bi}_2\text{Te}_3)_n$ heterostructure. The external magnetic field was applied perpendicular to the film plane (i.e., along the crystallographic c axis) (b) ^{55}Mn NMR frequency versus magnetic field applied in the c direction of MnBi_2Te_4 .

vestigated field range.

To understand the origin of these two signals we recall the basic NMR equation, determining the NMR frequency ω .

$$\omega = \gamma |\vec{B}_{\text{eff}}| \simeq \gamma |\vec{B}_{\text{hf}} + \vec{B}_{\text{ext}}| \quad (1)$$

where γ is the gyromagnetic ratio, characteristic for a specific nucleus and \vec{B}_{eff} denotes the strength of the effective magnetic field at the nucleus site, which in the absence of an external magnetic field is practically equal to the hyperfine field \vec{B}_{hf} .

The main contribution to hyperfine field comes from the contact Fermi term $\vec{B}_{\text{hf}}^{\text{cf}}$, which is due to the interaction of nuclear magnetic moment with the electronic magnetic moment of the same atom $\vec{B}_{\text{hf}}^{\text{cf,core}}$ and directed antiparallel to this moment. Therefore the respective upshift or downshift of the NMR frequency in presence of the external field is a fingerprint of antiparallel/parallel alignment of the magnetic moment vs. the field direction. In addition, magnetic moments of the surrounding atoms may also contribute to a hyperfine field, even on nuclei of non-magnetic ions, providing a transferred hyperfine field $\vec{B}_{\text{hf}}^{\text{cf,trans}}$ [31], which is typically at least one order of magnitude smaller than the on-site term:

$$\vec{B}_{\text{hf}}^{\text{cf}} = \vec{B}_{\text{hf}}^{\text{cf,core}} + \vec{B}_{\text{hf}}^{\text{cf,trans}} = A\mu_{\text{on-site}} + A'\Sigma\mu_s \quad (2)$$

where the A and A' denote the respective hyperfine interaction constants.

In view of the above, considering the morphology of our sample, we can readily attribute the main “black” ^{55}Mn NMR signal to the ferromagnetic component of the material, consisting of Mn layers in those SLs where the AFM coupling is not active. Indeed, as already pointed out, the majority of subsequent SLs are locked by the

AFM interaction, therefore in the absence of an external field they do not respond to the r.f. excitation and nuclear resonance is not observed from these parts of the sample. However, due to a non-uniform distribution of the QLs over the sample volume, some of the SLs are very distant from the next SL neighbor and their AFM coupling is very weak, if any. Therefore in presence of the weak external field these “loose” layers will easily align resulting in a steady rise of the macroscopic magnetization, as shown in Fig.1(b). The emerging unpinned magnetic moment is susceptible to r.f. excitation and is responsible for the onset of nuclear resonance, visible in the NMR spectra at and above 1.5 T.

An external magnetic field of around 3 T adds a new component to magnetization since the spin-flop transition entails the onset of a CAFM state. At this point the canted Mn moments contribute to the ^{55}Mn NMR giving rise to signal intensity. Enhancing the field strength even further, the Mn spins gradually rotate towards the field direction, increasing the magnetization component along the external field and reducing the effective field on nucleus, since the hyperfine field is oriented antiparallel to a local magnetic moment (eqn. 1). As a result, the NMR frequency decreases with increasing the external field, as observed in the experiment. As already mentioned, our sample reveals a certain distribution of the number of QLs separating the subsequent SLs, implying a distribution of their AFM coupling. Therefore, in the CAFM state the Mn magnetic moments reveal a certain orientation distribution and some of them will align at lower field values, while others require a stronger external field, evidenced by a long tail observed in the NMR spectra that were recorded in the presence of magnetic fields stronger than 3 T. Besides that, we cannot exclude a possible contribution to this signal from the Mn antisites embedded in QLs, which have been shown to couple ferromagnetically to the Mn layers within the SLs [20].

On the other hand, the upshifting “red” ^{55}Mn NMR signal is a fingerprint of some Mn magnetic moments that are clearly oriented opposite to the external field lower than 1.5 T, so the external field acts along the hyperfine field and the NMR frequency increases. These are the Mn_{Bi} antisites within the SLs – their antiparallel alignment with respect to the Mn planes has been already demonstrated in MnBi_2Te_4 by high-field magnetization measurements [30] and confirmed by NMR studies in the $\text{MnBi}_2\text{Te}_4/(\text{Bi}_2\text{Te}_3)_n$ system [32]. We note, however, that the observed frequency of the antisite ^{55}Mn NMR signal (around 419 MHz) differs from that reported in ref. [32] (around 470 MHz), which is likely due to a different form of the studied samples (our single crystal vs. polycrystalline samples studied in ref.[32]).

The individual antisite Mn moments are susceptible to the r.f. excitation and give the NMR signal even at zero field. As the external field gets stronger, they gradually align with the field adding to the magnetization of the uncoupled Mn layers, and contribute to the “black” spectrum component. Therefore the “red” signal even-

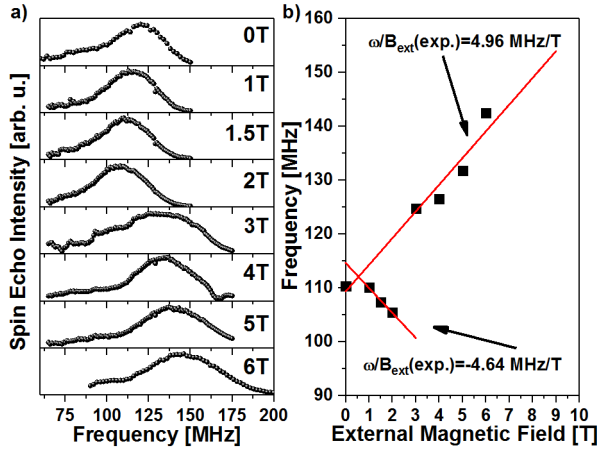


FIG. 3: (a) ^{209}Bi NMR spectra recorded at 4.2 K from an inhomogeneous $\text{MnBi}_2\text{Te}_4/(\text{Bi}_2\text{Te}_3)_n$ heterostructure. The external magnetic field was applied perpendicular to the film plane (i.e., along the crystallographic c axis) (b) ^{209}Bi NMR frequency versus magnetic field applied in the c direction of MnBi_2Te_4 .

tually disappears. The frequency position of the “black” NMR signal versus an external magnetic field (0-6 T), shows a quasi-linear decline with a slope of 8.5 MHz/T (Fig. 2(b)), confirming the magnetically non-saturated CAFM state of a sample. Indeed, by virtue of the eqn. 1 in the perfect antiparallel configuration of a hyperfine field vs. the external field, this slope would be equal to the gyromagnetic ratio $\gamma_{\text{Mn}} = 10.55 \text{ MHz/T}$. A smaller value means that only a component of an external field contributes to the effective local field on ^{55}Mn nucleus.

In addition to the ^{55}Mn NMR signals already discussed, at zero field we observe another strong NMR signal around 110 MHz. Whereas Mn is the only magnetic element in the system, the magnetic interactions can induce a magnetic moment on the otherwise non-magnetic elements, in this case Bi or Te. Considering the difference in the natural abundance of the respective isotopes $N = 100\%$ for ^{209}Bi (spin $I = 9/2$) vs. $N = 7\%$ for ^{125}Te (spin $I = 1/2$) the NMR signal intensity (expressed as $N(I + 1)I$) of bismuth is two orders of magnitude higher than that of Te. This means that the signal observed around 110 MHz can be undoubtedly attributed to ^{209}Bi nuclei. Taking into account the gyromagnetic ratio $\gamma_{\text{Bi}} = 6.84 \text{ MHz/T}$ we obtain that the effective field on ^{209}Bi amounts to around 16 T. This implies the presence of a magnetic moment induced by a hybridization of manganese 3d orbitals and bismuth valence 6p, 6s orbitals. Such moment has recently been reported from the x-ray magnetic circular dichroism study on a non-magnetic Se in the isostructural heterostruc-

tures $\text{MnBi}_2\text{Se}_4/(\text{Bi}_2\text{Se}_3)_n$ [33]. To the best of our knowledge, our observation of the ^{209}Bi NMR signal in the present study provides the first direct evidence that bismuth also reveals an induced magnetic moment in the $\text{MnBi}_2\text{Te}_4/(\text{Bi}_2\text{Te}_3)_n$ heterostructures.

We have further investigated this effect by recording the NMR spectra at different values of the external magnetic field applied along the [0001] direction (Fig. 3(a)). The frequency position of the ^{209}Bi NMR signal, plotted as a function of external magnetic field in the Fig. 3 (b), reveals above 2 T a linear dependence with the positive slope of 4.96 MHz/T. This is close to the ^{209}Bi gyromagnetic ratio $\gamma_{\text{Bi}} = 6.84 \text{ MHz/T}$, giving an additional proof for the correctness of our assignment of this signal to ^{209}Bi , rather than ^{125}Te ($\gamma_{\text{Te}} = 13.45 \text{ MHz/T}$).

Interestingly, the ^{209}Bi NMR spectra reveal a field dependence closely related to that observed for the antisite Mn_{Bi} signal. Just like in the case of a “red” ^{55}Mn NMR spectrum we can distinguish two field regimes: below 2 T the NMR frequency shifts towards lower frequencies while above 2 T a steady upshift is observed. This means that the induced magnetic moment on Bi is closely linked to manganese in the antisite Mn positions and oriented antiparallel to the parent Mn_{Bi} moment, which is located in the same atomic layer. Mn_{Bi} moment polarizes six bismuth nearest neighbors, so the effect is sixfold enhanced and gives rise to the observed strong ^{209}Bi NMR signal. It must be stressed that the straightforward attribution of the origin of Bi moment to the Mn_{Bi} antisites could only be possible based on the evolution of the ^{55}Mn and ^{209}Bi NMR spectra as a function of magnetic field with the well-defined, out-of-plane orientation.

To conclude: our NMR study performed on the self-organized single crystal $\text{MnBi}_2\text{Te}_4/(\text{Bi}_2\text{Te}_3)_n$ heterostructure as a function of the out-of-plane magnetic field up to 6 T demonstrates a pivotal role of the Mn_{Bi} antisites in modifying the magnetic interactions of this system. On one hand we confirm their AFM coupling to the main Mn layers at zero field, in agreement with previous theoretical and experimental reports [30, 32]. And more importantly, we demonstrate for the first time that they introduce a new magnetic moment to this system by polarizing the orbitals of bismuth. This moment is shown to be antiparallel to the moment of Mn antisites and thus parallel to the magnetic moment of the main Mn layers and as an additional ferromagnetic component of the system may be an important consideration in engineering the QAH devices.

R. K. was supported by The National Science Centre (NCN) grant 2022/06/X/ST3/00511.

[1] M. Mogi, M. Kawamura, A. Tsukazaki, R. Yoshimi, K. S. Takahashi, M. Kawasaki, and Y. Tokura, *Sci. Adv.* **3**, eaao1669 (2017).

[2] F. D. M. Haldane, *Phys. Rev. Lett.* **61**, 2015 (1988).
 [3] T. Hirahara, S. V. Eremin, T. Shirasawa, Y. O. nad T. Kubo, R. Nakanishi, R. Akiyama, A. Takayama,

- T. Hajiri, S. Ideta, M. Matsunami, K. Sumida, K. M. nad Y. Takagi, K. Tanaka, T. Okuda, T. Yokoyama, S. Kimura, S. Hasegawa, and E. V. Chulkov, *Nano Lett.* **17**, 3493 (2017).
- [4] C. Gong, L. Li, Z. Li, H. Ji, A. Stern, Y. Xia, T. Cao, W. Bao, C. Wang, Y. Wang, Z. Q. Qiu, R. J. Cava, S. G. Louie, J. Xia, and X. Zhang, *Nature* **546**, 265 (2017).
- [5] B. Huang, G. Clark, E. Navarro-Moratalla, D. R. Klein, R. Cheng, K. L. Seyler, D. Zhong, E. Schmidgall, M. A. McGuire, D. H. Cobden, W. Yao, D. Xiao, P. Jarillo-Herrero, and X. Xu, *Nature* **546**, 270 (2017).
- [6] Z. S. Aliev, I. R. Amiraslanov, D. I. Nasonova, A. V. Shevelkov, N. A. Abdullayev, Z. A. Jahangirli, E. N. Orujlu, M. M. Otrokov, N. T. Mamedov, M. B. Babanly, and E. V. Chulkov, *J. Alloy. Compd.* **789**, 443 (2019).
- [7] M. M. Otrokov, I. I. K. nad H. Bentmann, D. Estyunin, A. Zeugner, Z. S. Aliev, S. Gass, A. U. B. Wolter, A. V. Koroleva, A. M. Shikin, M. Blanco-Rey, M. Hoffmann, I. P. Rusinov, A. Y. Vyazovskaya, S. V. Ere-meev, Y. M. Koroteev, V. M. Kuznetsov, F. Freyse, J. Sanchez-Barriga, I. R. Amiraslanov, M. B. Babanly, N. T. Mamedov, N. A. Abdullayev, V. N. Zverev, A. Alfonso, V. Kataev, B. Buchner, E. F. Schwier, S. Kumar, A. Kimura, L. Petaccia, G. D. Santo, R. C. Vidal, S. Schatz, K. Kissner, M. Unzelmann, C. H. Min, S. Moser, T. R. F. Peixoto, F. Reinert, A. Ernst, P. M. Echenique, A. Isaeva, and E. V. Chulkov, *Nature* **576**, 416 (2019).
- [8] M. M. Otrokov, I. P. Prusinov, M. Blanco-Rey, M. Hoffmann, A. Y. Vyazovskaya, S. V. Ere-meev, A. Ernst, P. M. Echenique, A. Arnau, and E. V. Chulkov, *Phys Rev. Lett.* **122**, 107202 (2019).
- [9] Y. Gong, J. Guo, J. Li, K. Zhu, M. Liao, X. Liu, Q. Zhang, L. Gu, L. Tang, X. Feng, D. Zhang, W. Li, C. Song, L. Wang, P. Yu, X. Chen, Y. Wang, H. Yao, W. Duan, Q.-K. Xue, and K. He, *Chinese Phys. Lett.* **36**, 076801 (2019).
- [10] J. Li, Y. Li, S. Du, Z. Wang, B.-L. Gu, S.-C. Zhang, K. He, W. Duan, and Y. Xu, *Sci. Adv.* **5**, eaaw5685 (2019).
- [11] B. Li, J.-Q. Yan, D. M. Pajerowski, E. Gordon, A.-M. Nedić, Y. Sizyuk, L. Ke, P. P. Orth, D. Vaknin, and R. J. McQueeney, *Phys. Rev. Lett.* **124**, 167204 (2020).
- [12] K. He, *npj Quantum Mater.* **5**, 90 (2020).
- [13] G. Akhgar, Q. Li, I. D. Bernardo, C. X. Trang, C. Liu, A. Zavabeti, J. Karel, A. Tadich, M. S. Fuhrer, and M. T. Edmonds, *ACS Appl. Mater. Interfaces* **14**, 6102 (2022).
- [14] R. Gao, G. Qin, S. Qi, Z. Qiao, and W. Ren, *Phys. Rev. Mater.* **5**, 114201 (2021).
- [15] D. S. Lee, T.-H. Kim, C.-H. Park, C.-Y. Chung, Y. S. Lim, W. S. Seo, and H.-H. Park, *Cryst. Eng. Comm.* **15**, 5532 (2013).
- [16] I. I. Klimovskikh, M. M. Otrokov, D. Estyunin, S. V. Ere-meev, S. O. Filnov, A. Koroleva, E. Shevchenko, V. Voroshnin, A. G. Rybkin, I. P. Rusinov, M. Blanco-Rey, M. Hoffmann, Z. S. Aliev, M. B. Babanly, I. R. Amiraslanov, N. A. Abdullayev, V. N. Zverev, A. Kimura, O. E. Tereshchenko, K. A. Kokh, L. Petaccia, G. D. Santo, A. Ernst, P. M. Echenique, N. T. Mamedov, A. M. Shikin, and E. V. Chulkov, *npj Quantum Mater.* **5**, 54 (2020).
- [17] J. Wu, F. Liu, C. Liu, Y. Wang, C. Li, Y. Lu, S. Matsushii, and H. Hosono, *Adv. Mater.* **32**, 2001815 (2020).
- [18] K. Y. Chen, B. S. Wang, J.-Q. Yan, D. S. Parker, J.-S. Zhou, Y. Uwatoko, and J.-G. Cheng, *Phys. Rev. Mater.* **3**, 094201 (2019).
- [19] S. H. Lee, Y. Zhu, Y. Wang, L. Miao, T. Pillsbury, H. Yi, S. Kempinger, J. Hu, C. A. Heikes, P. Quarterman, W. Ratcliff, J. A. Borchers, H. Zhang, X. Ke, D. Graf, N. Alem, C.-Z. Chang, N. Samarth, and Z. Mao, *Phys. Rev. Res.* **1**, 012011(R) (2019).
- [20] J. Sitnicka, K. Park, P. Skupiński, K. Graszka, A. Reszka, K. Sobczak, J. Borysiuk, Z. Adamus, M. Tokarczyk, A. Avdonin, I. Fedorchenko, I. Abaloszewa, S. Turczyniak-Surdacka, N. Olszowska, J. Kolodziej, B. J. Kowalski, H. Deng, M. Konczykowski, L. Krusin-Elbaum, and A. Wolos, *2D Mater.* **9**, 015026 (2022).
- [21] Z. Huang, M.-H. Du, J. Yan, and W. Wu, *Phys. Rev. Mater.* **4**, 121202(R) (2020).
- [22] F. Islam, Y. Lee, D. M. Pajerowski, J. Oh, W. Tian, L. Zhou, J. Yan, L. Ke, R. J. McQueeney, and D. Vaknin, *Adv. Mater.* **35**, 2209951 (2023).
- [23] K. Momma and F. Izumi, *J. Appl. Crystallogr.* **44**, 1272 (2011).
- [24] S. Nadolski, M. Wójcik, E. Jedryka, and K. Nesteruk, *J. Magn. Magn. Mater.* **140**, 2187 (1995).
- [25] P. Panissod, M. Malinowska, E. Jedryka, M. Wójcik, S. Nadolski, M. Knobel, and J. E. Schmidt, *Phys. Rev. B* **63**, 014408 (2000).
- [26] J.-Q. Yan, Q. Zhang, T. Heitmann, Z. Huang, K. Y. Chen, J.-G. Cheng, W. Wu, D. Vaknin, B. C. Sales, and R. J. McQueeney, *Phys. Rev. Mater.* **3**, 064202 (2019).
- [27] Y. Liu, L.-L. Wang, Q. Zheng, Z. Huang, X. Wang, M. Chi, Y. Wu, B. C. Chakoumakos, M. A. McGuire, B. C. Sales, W. Wu, and J. Yan, *Phys. Rev. X* **11**, 021033 (2021).
- [28] X. Wu, C. Ruan, P. Tang, F. Kang, W. Duan, and J. Li, *Nano Lett.* **23**, 5048 (2023).
- [29] C. Yan, Y. Zhu, L. Miao, S. Fernandez-Mulligan, E. Green, R. Mei, H. Tan, B. Yan, C.-X. Liu, N. Alem, Z. Mao, and S. Yang, *Nano Lett.* **22**, 9815 (2022).
- [30] Y. Lai, L. Ke, J. Yan, R. D. McDonald, and R. J. McQueeney, *Phys. Rev. B* **103**, 184429 (2021).
- [31] E. Jedryka and M. Wójcik, Nuclear magnetic resonance in nanomagnetic systems, in *Nanomagnetic Materials, Fabrication, Characterization and Application*, edited by A. Yamaguchi, A. Hirohata, and B. J. Stadler (Elsevier, 2021).
- [32] M. Sahoo, I. J. Onuorah, L. C. Folkers, E. Kochetkova, E. V. Chulkov, M. M. Otrokov, Z. S. Aliev, I. R. Amiraslanov, A. U. B. Wolter, B. Büchner, L. T. Corredor, C. Wang, Z. Salman, A. Isaeva, R. D. Renzi, and G. Al-lodi, *Adv. Sci.* **11**, 2402753 (2024).
- [33] R. Fukushima, V. N. Antonov, M. M. Otrokov, T. T. Sasaki, R. Akiyama, K. Sumida, K. Ishihara, S. Ichinokura, K. Tanaka, Y. Takeda, D. P. Salinas, S. V. Ere-meev, E. V. Chulkov, A. Ernst, and T. Hirahara, *Phys. Rev. Mater.* **8**, 084202 (2024).